

Article

# BRISENT: An Entropy-Based Model for Bridge-Pier Scour Estimation under Complex Hydraulic Scenarios

Alonso Pizarro <sup>1,\*</sup> , Caterina Samela <sup>1</sup> , Mauro Fiorentino <sup>1</sup>, Oscar Link <sup>2</sup> and Salvatore Manfreda <sup>1</sup>

<sup>1</sup> Department of European and Mediterranean Cultures, Università degli Studi della Basilicata, Potenza 85100, Italy; caterina.samela@unibas.it (C.S.); mauro.fiorentino@unibas.it (M.F.); salvatore.manfreda@unibas.it (S.M.)

<sup>2</sup> Department of Civil Engineering, Universidad de Concepción, Concepción 4030000, Chile; olink@udec.cl

\* Correspondence: alonso.pizarro@unibas.it; Tel.: +39-389-280-4201

Received: 21 September 2017; Accepted: 8 November 2017; Published: 14 November 2017

**Abstract:** The goal of this paper is to introduce the first clear-water scour model based on both the informational entropy concept and the principle of maximum entropy, showing that a variational approach is ideal for describing erosional processes under complex situations. The proposed bridge–pier scour entropic (BRISENT) model is capable of reproducing the main dynamics of scour depth evolution under steady hydraulic conditions, step-wise hydrographs, and flood waves. For the calibration process, 266 clear-water scour experiments from 20 precedent studies were considered, where the dimensionless parameters varied widely. Simple formulations are proposed to estimate BRISENT’s fitting coefficients, in which the ratio between pier-diameter and sediment-size was the most critical physical characteristic controlling scour model parametrization. A validation process considering highly unsteady and multi-peaked hydrographs was carried out, showing that the proposed BRISENT model reproduces scour evolution with high accuracy.

**Keywords:** sediment transport; bridge scour; informational entropy; principle of maximum entropy; effective flow work; unsteady hydraulic conditions

## 1. Introduction

Bridges are important for society because they allow social, cultural, and economic connectivity; as such, they are key pieces in the development process and progress. At the same time, bridges continually suffer the action of natural hazards which exposes the road network to risk. The main cause of bridge collapse is related to hydraulic conditions [1–6], where flood events can compromise the safety of the whole structure, including its failure. Therefore, the pier-scour phenomenon has become a subject of research for civil and environmental engineers who have proposed many formulas in this field (see e.g., [7–10]).

Estimating the maximum scour depth around bridge piers and its temporal evolution is a critical step in the design of foundations. Previous researchers have proposed formulas to reproduce the time-dependent scour depth and its maximum value. Among them, Zanke [10] proposed a semi-empirical formulation based on the principle of mass conservation of the bedload. Richardson and Davis [8] used literature data generated by several authors to develop the well-known HEC-18 scour equation, later extended for wide piers. Manes and Brocchini [11] proposed a novel approach combining theoretical arguments with considerations taken from empirical evidence in order to provide new avenues for the development of general predictive models founded more on physical than empirical grounds. Dey [12] elaborated a theoretical model, considering that the key agent in the scour process is the horseshoe vortex. Melville and Chiew [13] and Oliveto and Hager [14]

developed empirical scour formulas, where a logarithmic relationship between time and scour-depth was assumed. Subsequently, the Sheppard and Miller [15] and Melville [7] equations were combined and slightly modified in order to form a new scour equation: the Sheppard and Melville (S/M) equation [9]. Although the aforementioned scour models are valid under steady hydraulic conditions, they could be used with stepwise hydrographs adopting the convolution technique (see e.g., [16–19]). Such technique relies on the superposition concept that allows the consideration of a hydrograph as a sequence of steady discharge steps, in which steady scour models are valid.

Other efforts have been made to explain the bridge scour process under 100% unsteady hydraulic conditions. In this context, Lai et al. [16] examine the rising limb of a triangular hydrograph, introducing an unsteady flow parameter combining peak flow intensity and time-to-peak factors. The effect of a single-peaked flood wave on pier scour was investigated by Hager and Unger [20], who defined the hydrograph by its time to peak and peak discharge. Recently, Pizarro et al. [21] proposed the dimensionless effective flow work parameter  $W^*$  for treating bridge scour phenomena under several different hydraulic conditions, showing that multiple peak hydrographs can be analyzed and well represented through  $W^*$ . Link et al. [22] proposed the dimensionless effective flow work (DFW) model for evaluating the time-dependent scour-depth under flood waves based on such dimensionless effective flow work.

Furthermore, efforts to monitor real bridge piers have been reported by Sturm et al. [23], Clubley et al. [24], Prendergast and Gavin [25], Hong et al. [26], Su and Lu [27] and others. In particular, Sturm et al. [23] carried out field measurements, laboratory modeling, and 3D numerical modeling of bridge scour. Their field data consisted of a continuous measurement of velocity and scour depth during real flood events, highlighting the scour-hole refilling aspect of the process and the difficulties in scaling the physically modeled scour depth from laboratory to field.

In addition, by applying bridge-scour formulas that take into account constant sediment properties, hydraulic conditions, and pier geometry, the results obtained vary considerably [9]. In this regard, using both field datasets and synthetic data, Gaudio et al. [28] showed that with certain input parameters, different predictions are expected from various bridge scour equations. In another study, Gaudio et al. [29] concluded that the sensitivity of the bridge scour equations to the influencing parameters is not a certain value for all the equations. Hence, various predictions may result using different equations. Therefore, the application of current scour models is restricted to idealized conditions and involves important uncertainties in real cases with complex hydraulic scenarios and natural regimes. Overestimation of scour depth may result in unnecessary costs while, on the other hand, an underestimation imprudently increases the risk of failure of the bridge, loss of life, and connectivity problems. Erosional processes are complex to treat mathematically due to the inherent interaction at different spatial scales. For instance, bridge scour is a local phenomenon that interacts with channel instability, channel bed gradation, channel migration, and contraction scour, which act simultaneously. Consequently, the final response of the bridge depends on the sum of these loads, where the uncertainties of each river process are propagated and accumulated. The issue of quantifying bridge scour uncertainties has already been studied by Barbe et al. [30], Johnson [31,32], Johnson and Ayyub [33,34], Johnson and Hell [35], Johnson and Dock [36], Yanmaz and Cicekdag [37], Yanmaz and Üstün [38], Johnson et al. [39] and others.

Despite previous, enormous efforts, there is still much to do in the field of scour research. For example, recent advances on scour collapse-inducing flow return periods show that their values are considerably scattered, with a range of between one to more than 1000 years [40]. Therefore, linking bridge collapse to a single return period discharge does not provide reliable information on the scour process. Additionally, the potential consequences of climate change on precipitation patterns, catchment characteristics, and river flow characteristics lead to increased uncertainties on bridge scour performances, which are currently unknown.

In this context, informational entropy has long been recognized as a measure of these uncertainties (see e.g., [41–45]) and it is the ideal concept to analyze them in the presence of erosional processes.

The goal of this paper is to introduce the first scour model based on both the informational entropy concept and the principle of maximum entropy (POME), showing that a variational approach is ideal for describing erosional processes under complex hydraulic situations.

The paper is organized as follows: first, the informational entropy concept and POME are introduced; the BRISENT model is then formulated and presented in detail; literature data for the model test are described; the calibration/estimation of model parameters is presented and discussed; and the BRISENT model is validated with multi-peaked hydrographs containing sequences of flood events. Conclusions are drawn at the end.

## 2. The Informational Entropy Concept

The informational entropy concept and its theory have been applied before in statistical mechanics, information theory, hydrology, and water resources (e.g., [46–53]), providing good results and an easy way to introduce probabilities into hydraulics. Informational entropy, Shannon entropy or simple entropy is defined in terms of probability. Taking into account the continuous random variable  $\underline{X}$ , entropy is defined as:

$$\Phi(\underline{X}) := - \int_{-\infty}^{\infty} f(X) \ln f(X) dX = E[-\ln f(\underline{X})], \quad (1)$$

in which  $\Phi(\underline{X})$  is the entropy,  $f(X)$  is the probability density function of  $\underline{X}$ , and  $E[\ ]$  denotes expectation. Note that for random variable notation, the Dutch convention is adopted [54] according to which a random variable is underlined.

Informational entropy may be considered a measure of the uncertainties as well as a quantity of information contained in the data [43]. Theoretically, a uniform probability distribution maximizes the entropy defined in Equation (1) [47]; however, due to the constraints that define the physics of different phenomena, the probability density function is not always uniform. According to Chiu [47], the entropy concept can be thought of as a measure of how close the real probability density function is to the uniform function. Therefore, a maximization of entropy will make the probability density function as uniformly as possible, considering the constraints. In this context, and from a physical perspective, the tendency toward maximal entropy is the driving force of natural change, where POME is the logic counterpart of the second law of thermodynamics [43,46].

The maximization of entropy to determine  $f(X)$  may be resolved using the method of variational calculus. Maximizing Equation (1) and satisfying the “ $n$ ” constraints defined in Equation (2) is equivalent to maximizing the Lagrange function presented in Equation (3):

$$\phi_i(X, f(X)) = C_i, \quad i = 1, 2, 3, \dots, n, \quad (2)$$

$$L(f(X), \lambda_i) = \Phi(\underline{X}) - \sum_{i=1}^n \lambda_i \{ \phi_i(X, f(X)) - C_i \}, \quad (3)$$

in which  $\lambda_i$  are the Lagrange multipliers and  $i$  is the number of constraints. Thus, the mathematical function of  $f(X)$  can be obtained by solving Equation (4) and therefore, a simple function of  $\underline{X}$  can be deduced,

$$\frac{\partial L(f(X), \lambda_i)}{\partial f(X)} = \frac{\partial \Phi(\underline{X})}{\partial f(X)} - \sum_{i=1}^n \lambda_i \frac{\partial \phi_i(X, f(X))}{\partial f(X)} = 0 \quad (4)$$

## 3. The BRISENT Model

The dimensionless, effective flow work by the flow on the streambed around a pier,  $W^*$ , was deduced from dimensional analysis and physical considerations by Pizarro et al. [21]:

$$W^*(t_{con}) = \int_0^{t_{con}} \frac{1}{t_R} \left( \frac{u(t) - 0.5u_c}{u_R} \right)^4 \delta dt \quad (5)$$

where  $t_{con}$  is the considered time,  $t_R$  is a reference time ( $= z_R/u_R$ ),  $z_R = D^2/2d_{50}$  is a reference length ( $D$  is the pier-diameter and  $d_{50}$  the sediment-size),  $u$  is the section averaged flow velocity,  $u_R$  is a reference velocity ( $= \sqrt{\rho'gd_{50}}$ , where  $\rho' = (\rho_S - \rho_W)/\rho_W$  is the relative density between sediment “s” and water “w”, and  $g$  is the gravitational acceleration).  $u_c$  is the critical flow velocity for incipient motion of sediment particles. Based on experimental evidence (e.g., [10,55–57]), it is considered that scour occurs when  $u(t) \geq 0.5u_c$ , thus:

$$\delta = \begin{cases} 0, & u(t)/u_c < 0.5 \\ 1, & u(t)/u_c \geq 0.5 \end{cases} \quad (6)$$

$W^*$  is an energetic parameter applied to local scour phenomena. Consequently, POME applied to  $W^*$  results in a variational/thermodynamic approach for treating the local scour process.

Pizarro et al. [21] evidenced that under constant sediment properties, geometrical scale, and clear-water conditions the mathematical relation between the relative scour depth  $Z^*$  and  $W^*$  is unique.  $Z^* = z/z_R$  is defined as a normalized parameter, where  $z$  is the dimensional scour depth and  $z_R$  the reference length established previously. In agreement with Link et al. [22],  $Z^*$  increases monotonously over  $W^*$ , taking values from zero at non-eroded conditions to a maximum value at the equilibrium state. Based on the Laplace principle of insufficient reason and therefore, assuming that all values of  $W^*$  between zero and a maximum considered value,  $W_{max}^*$  are equally likely to be attached (not necessarily true), then the probability of the relative scour depth to be equal to or less than  $Z^*$ ,  $Pr(\underline{Z}^* \leq Z^*) = F(Z^*)$ , can be specified by  $W^*/W_{max}^*$ . Thus,

$$F(Z^*) = \frac{W^*}{W_{max}^*}, \quad (7)$$

and the probability density function of  $\underline{Z}^*$  is the derivative of Equation (7):

$$f(Z^*) = \frac{\partial F(Z^*)}{\partial Z^*} = \frac{1}{W_{max}^*} \frac{\partial W^*}{\partial Z^*}, \quad (8)$$

Unfortunately, Equation (8) cannot be used to determine  $f(Z^*)$  because the derivate of  $W^*$  over  $Z^*$  is unknown. However, POME can be exploited for this purpose. Equation (9) reveals the informational entropy applied to the scour phenomenon:

$$\Phi(\underline{Z}^*) = - \int_0^{Z_{max}^*} f(Z^*) \ln f(Z^*) dZ^*, \quad (9)$$

Resolving the issue to find the probability density function of  $\underline{Z}^*$  implies using Equation (9) with a few constraints that completely define the boundary conditions and physics. The first constraint must satisfy the axiom of probability:

$$\int_0^{Z_{max}^*} f(Z^*) dZ^* = 1, \quad (10)$$

and the second constraint, related to the mass conservation law for bridge-pier scour phenomenon at equilibrium condition, can be written as:

$$\int_0^{Z_{max}^*} Z^* f(Z^*) dZ^* = \overline{Z^*}, \quad (11)$$

in which  $\overline{Z^*}$  is the ( $W^*$ -averaged) mean relative scour depth, i.e., the average value of  $Z^*$  during the scour process.

The scour entropy given by Equation (9) needs to be maximized subjected to the constraints in Equations (10) and (11). For this purpose, the method of Lagrange multipliers is adopted. The probability density function  $f(Z^*)$  is:

$$f(Z^*) = \exp(\lambda_1 - 1) \exp(\lambda_2 Z^*), \quad (12)$$

where  $\lambda_1$  and  $\lambda_2$  are Lagrange multipliers. After substitution of Equation (12) into the constraint equations, and considering the boundary condition  $Z^* = 0$  at  $W^* = 0$ , the final equations after some algebra are:

$$S = \lambda Z_{max}^*, \quad (13)$$

$$Z^* = \frac{1}{\lambda} \ln \left\{ 1 + \frac{W^*}{W_{max}^*} [\exp(S) - 1] \right\}, \quad (14)$$

$$\bar{Z}^* = \frac{Z_{max}^* \exp(S)}{\exp(S) - 1} - \frac{1}{\lambda}, \quad (15)$$

$$f(Z^*) = \frac{\lambda \exp(\lambda Z^*)}{\exp(S) - 1}, \quad (16)$$

$$F(Z^*) = \frac{\exp(\lambda Z^*) - 1}{\exp(S) - 1}, \quad (17)$$

in which  $Z_{max}^* = \max(Z^*)$  is the maximum relative scour depth associated to the maximum dimensionless, effective flow work  $W_{max}^* = \max(W^*)$ ,  $\lambda = \lambda_2$  is a Lagrange multiplier that needs to be estimated, and  $S$  is defined as the entropic-scour parameter. Note that due to the physical relationship between  $W_{max}^*$  and  $Z_{max}^*$ , the BRISENT model contains two fitting parameters:  $\lambda$  and  $Z_{max}^*$ . These parameters depend on scour influencing parameters and can be estimated as described in the following sections.

## 4. Methods

### 4.1. Data Characterization for $\lambda$ Estimation

Experimental data were compiled from available studies in Chabert and Engeldinger [58], Zanke [10], Franzetti et al. [59], Oliveto and Hager [14,19], Sheppard et al. [60], Grimaldi [61], Alabi [62], Simarro et al. [63], Meyering [64], Lança et al. [65], Link et al. [22] and Pizarro et al. [21]. Altogether, results corresponding to 137 experiments were analyzed. Experimental conditions of scour experiments are presented in Table 1 in which  $t$  is the experimental time,  $D^* = d_{50}(\rho'g/v^2)^{\frac{1}{3}}$  is the dimensionless particle diameter,  $v$  is the kinematic viscosity,  $D/d_{50}$  is the ratio between pier-diameter and sediment-size,  $h/D$  is the ratio between flow-depth and pier-diameter, and  $u/u_c$  is the flow intensity.

Note that for run names a standard notation was selected in order to provide a simple and characteristic code that contains the year of publication, author names, number of experiment, and its hydraulic conditions. For example, "2017PIZARRO05U" is the unsteady experiment number 5 carried out by Pizarro et al. [21] and "2004SHEPPARD04S" is the steady experiment number 4 performed by Sheppard et al. [60].

The scour data in Table 1 can be classified as steady or unsteady, depending on the hydraulic conditions in which the experiments were performed. For time-dependent runs, the flow-discharge, flow-velocity, and flow-depth vary in time, whereas the values presented in Table 1 refer to peak flow conditions. Figure 1 shows the hydrographs corresponding to the 14 unsteady runs considered herein. Stepwise hydrographs are presented in Figure 1j–l.

**Table 1.** Characterization of the experimental data employed for  $\lambda$  estimation.

Authors	Run	$d_{50}$ (mm)	$t$ (Days)	$D^*$	$\rho'$	$D/d_{50}$	$h/D$	$u/u_c$
Chabert and Engeldinger [58]	1956CHABERT01S	0.26	4.29	6.58	1.65	192.26	4.00	0.75
	1956CHABERT02S	0.26	4.29	6.58	1.65	288.46	2.67	0.75
	1956CHABERT03S	0.26	4.29	6.58	1.65	384.62	2.00	0.75
	1956CHABERT04S	0.26	3.92	6.58	1.65	192.26	7.00	0.92
	1956CHABERT05S	0.26	3.92	6.58	1.65	288.46	4.67	0.92
	1956CHABERT06S	0.26	3.92	6.58	1.65	384.62	3.50	0.92
	1956CHABERT07S	0.26	0.55	6.58	1.65	192.26	2.00	1.20
	1956CHABERT08S	0.52	6.75	13.15	1.65	96.13	2.00	1.52
	1956CHABERT09S	1.50	5.29	37.94	1.65	33.32	2.00	0.97
	1956CHABERT10S	1.50	5.29	37.94	1.65	66.67	1.00	0.97
	1956CHABERT11S	1.50	5.29	37.94	1.65	100.00	0.67	0.97
	1956CHABERT12S	1.50	1.68	37.94	1.65	33.32	4.00	0.69
	1956CHABERT13S	1.50	1.68	37.94	1.65	66.67	2.00	0.69
	1956CHABERT14S	1.50	1.68	37.94	1.65	100.00	1.33	0.69
	1956CHABERT15S	1.50	7.29	37.94	1.65	33.32	7.00	0.74
	1956CHABERT16S	1.50	7.29	37.94	1.65	66.67	3.50	0.74
	1956CHABERT17S	1.50	7.29	37.94	1.65	100.00	2.33	0.74
Zanke [10]	1982ZANKE01S	0.24	0.002	5.84	1.65	375.00	4.67	0.75
Franzetti et al. [59]	1989FRANZETTI01S	2.50	58.13	30.22	0.18	19.20	3.00	0.79
Oliveto and Hager [14,19]	2002OLIVETO01S	0.55	0.04	13.91	1.65	200.00	1.40	0.96
	2002OLIVETO02S	0.55	0.93	13.91	1.65	200.00	1.35	0.70
	2002OLIVETO03S	0.55	0.44	13.91	1.65	200.00	2.75	0.66
	2002OLIVETO04S	0.55	21.06	13.91	1.65	200.00	1.82	0.62
	2002OLIVETO05S	0.55	0.20	13.91	1.65	116.36	2.32	0.62
	2002OLIVETO06S	0.55	0.03	13.91	1.65	116.36	3.13	0.70
	2002OLIVETO07S	0.55	0.89	13.91	1.65	116.36	4.69	0.66
	2002OLIVETO08S	0.55	2.94	13.91	1.65	467.27	0.39	0.64
	2002OLIVETO09S	0.55	0.22	13.91	1.65	467.27	0.38	0.79
	2002OLIVETO10S	0.55	1.89	13.91	1.65	467.27	1.17	0.59
	2002OLIVETO11S	3.30	3.95	52.90	0.42	15.17	4.99	0.83
	2002OLIVETO12S	3.30	1.85	52.90	0.42	15.17	2.95	0.73
	2002OLIVETO13S	3.30	0.96	52.90	0.42	15.17	1.00	0.84
	2002OLIVETO14S	3.30	0.88	52.90	0.42	33.33	1.36	0.90
	2002OLIVETO15S	3.30	46.88	52.90	0.42	33.33	0.96	0.87
	2002OLIVETO16S	3.30	0.71	52.90	0.42	33.33	0.45	1.00
	2002OLIVETO17S	3.30	2.71	52.90	0.42	33.33	0.90	0.77
	2002OLIVETO18S	3.30	0.92	52.90	0.42	33.33	0.94	1.13
	2002OLIVETO19S	3.30	0.88	52.90	0.42	77.88	0.58	0.70
	2002OLIVETO20S	3.30	0.96	52.90	0.42	77.88	0.19	0.84
	2002OLIVETO21S	3.30	2.92	52.90	0.42	77.88	0.16	0.66
	2002OLIVETO22S	4.80	0.95	121.42	1.65	13.23	2.41	0.94
	2002OLIVETO23S	4.80	0.92	121.42	1.65	13.23	3.19	0.73
	2002OLIVETO24S	4.80	0.95	121.42	1.65	13.23	2.42	0.84
	2002OLIVETO25S	4.80	0.76	121.42	1.65	13.23	1.58	0.68
	2002OLIVETO26S	4.80	0.92	121.42	1.65	22.92	0.85	0.98
	2002OLIVETO27S	4.80	0.59	121.42	1.65	22.92	0.87	0.74
	2002OLIVETO28S	4.80	1.13	121.42	1.65	53.54	0.18	0.97
	2002OLIVETO29S	4.80	0.10	121.42	1.65	53.54	0.20	0.75
	2002OLIVETO30S	4.80	1.87	121.42	1.65	53.54	0.21	0.54
	2002OLIVETO31S	4.80	0.46	121.42	1.65	104.17	0.12	0.68
	2002OLIVETO32S	3.10	1.75	78.42	1.65	35.48	0.92	0.76
	2002OLIVETO33S	3.10	0.13	78.42	1.65	35.48	0.78	1.14
2005OLIVETO01U	3.10	0.04	78.42	1.65	35.48	1.40	0.70	
2005OLIVETO02U	3.10	0.03	78.42	1.65	35.48	1.57	0.76	
2005OLIVETO03U	3.10	0.03	78.42	1.65	35.48	1.69	0.87	
2005OLIVETO04U	3.10	0.02	78.42	1.65	35.48	1.53	0.81	
2005OLIVETO05U	3.10	0.06	78.42	1.65	35.48	1.52	0.81	
2005OLIVETO06U	3.10	0.05	78.42	1.65	35.48	1.45	0.84	

Table 1. Cont.

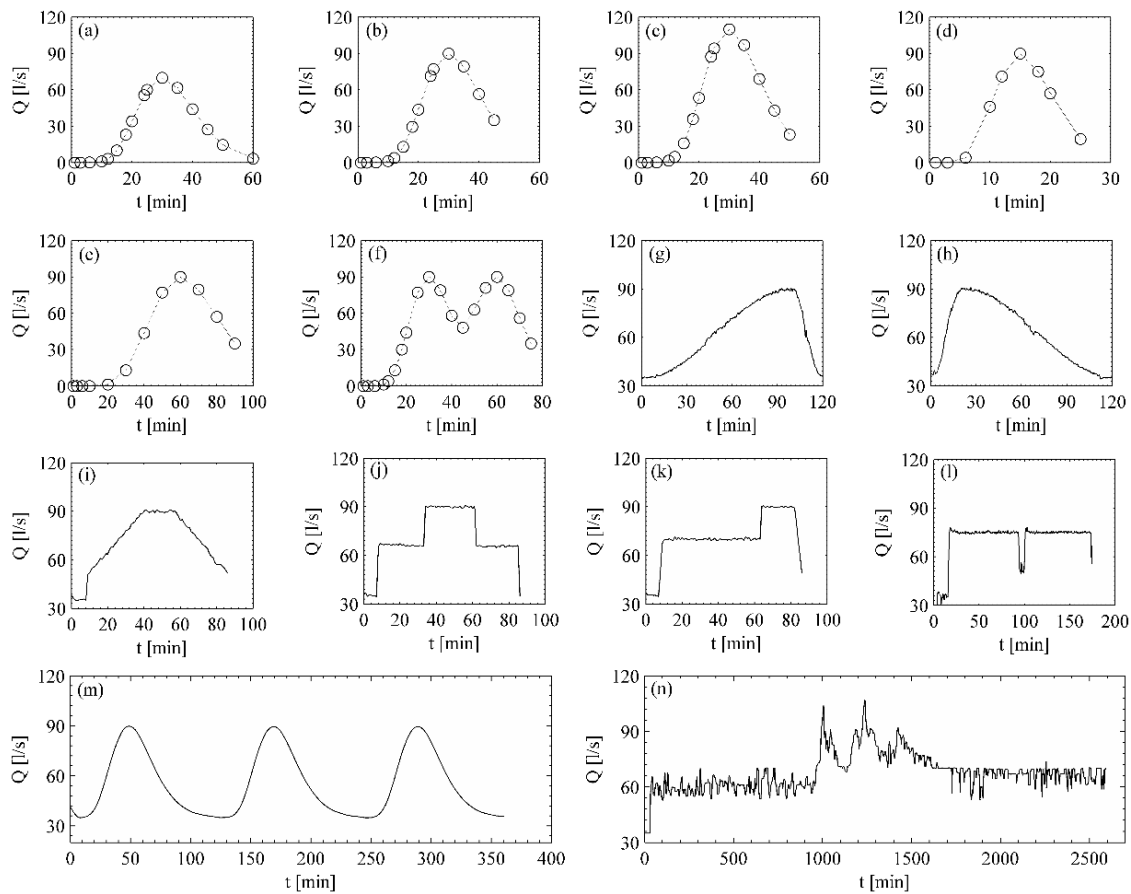
Authors	Run	$d_{50}$ (mm)	$t$ (Days)	$D^*$	$\rho'$	$D/d_{50}$	$h/D$	$u/u_c$
Sheppard et al. [60]	2004SHEPPARD01S	0.22	3.71	5.57	1.65	518.18	10.44	0.91
	2004SHEPPARD02S	0.22	6.79	5.57	1.65	1386.36	3.90	0.97
	2004SHEPPARD03S	0.80	15.00	20.24	1.65	1143.75	1.39	0.85
	2004SHEPPARD04S	0.80	5.96	20.24	1.65	1143.75	0.95	0.87
	2004SHEPPARD05S	0.80	3.67	20.24	1.65	381.25	4.16	0.83
	2004SHEPPARD06S	0.80	1.71	20.24	1.65	142.50	11.14	0.87
	2004SHEPPARD07S	2.90	7.83	73.36	1.65	315.52	1.33	0.90
	2004SHEPPARD08S	2.90	13.75	73.36	1.65	315.52	0.61	0.84
	2004SHEPPARD09S	2.90	18.67	73.36	1.65	315.52	0.32	0.83
	2004SHEPPARD10S	2.90	25.67	73.36	1.65	315.52	0.19	0.76
	2004SHEPPARD11S	0.22	24.17	5.57	1.65	4159.09	1.98	0.94
Grimaldi [61]	2005GRIMALDI01S	1.28	4.00	32.38	1.65	58.59	2.00	1.00
	2005GRIMALDI02S	0.86	6.16	21.75	1.65	104.65	2.78	1.00
	2005GRIMALDI03S	0.86	6.09	21.75	1.65	139.53	2.08	1.00
Alabi [62]	2006ALABI01S	0.53	3.29	13.41	1.65	216.98	2.00	0.89
	2006ALABI02S	0.53	2.04	13.41	1.65	137.74	2.05	0.89
	2006ALABI03S	0.53	22.13	13.41	1.65	216.98	2.00	0.70
Simarro et al. [63]	2011SIMARRO01S	0.86	34.90	21.75	1.65	87.21	2.13	0.88
	2011SIMARRO02S	0.86	45.60	21.75	1.65	93.02	2.00	0.94
	2011SIMARRO03S	1.28	29.73	32.38	1.65	62.50	2.00	0.93
	2011SIMARRO04S	1.28	24.85	32.38	1.65	58.59	2.00	0.93
	2011SIMARRO05S	1.28	28.99	32.38	1.65	49.22	2.06	0.93
Meyering [64]	2012MEYERING01S	0.20	10.00	5.06	1.65	150.00	3.33	1.00
	2012MEYERING02S	0.80	10.00	20.24	1.65	37.50	3.33	1.00
	2012MEYERING03S	1.60	10.00	40.47	1.65	18.75	3.33	1.00
	2012MEYERING04S	2.50	10.00	63.24	1.65	12.00	3.33	1.00
	2012MEYERING05S	2.60	10.00	40.66	0.39	11.54	3.33	1.00
	2012MEYERING06S	2.70	10.00	19.77	0.04	11.11	3.33	1.00
	2012MEYERING07S	2.00	0.42	17.64	0.07	12.50	13.20	1.00
	2012MEYERING08S	2.00	0.42	17.64	0.07	25.00	6.60	1.00
	2012MEYERING09S	2.00	0.42	17.64	0.07	35.00	4.71	1.00
Lança et al. [65]	2013LANÇA01S	0.86	7.08	21.75	1.65	127.91	0.50	0.97
	2013LANÇA02S	0.86	7.00	21.75	1.65	186.05	0.50	0.97
	2013LANÇA03S	0.86	7.08	21.75	1.65	232.56	0.50	0.97
	2013LANÇA04S	0.86	7.00	21.75	1.65	290.70	0.50	0.97
	2013LANÇA05S	0.86	9.29	21.75	1.65	366.28	0.50	0.93
	2013LANÇA06S	0.86	12.75	21.75	1.65	406.98	0.50	1.00
	2013LANÇA07S	0.86	12.00	21.75	1.65	465.12	0.50	0.96
	2013LANÇA08S	0.86	7.00	21.75	1.65	58.14	1.00	0.97
	2013LANÇA09S	0.86	7.00	21.75	1.65	87.20	1.00	0.97
	2013LANÇA10S	0.86	7.00	21.75	1.65	127.91	1.00	0.97
	2013LANÇA11S	0.86	11.88	21.75	1.65	186.05	1.00	0.95
	2013LANÇA12S	0.86	10.88	21.75	1.65	232.60	1.00	0.96
	2013LANÇA13S	0.86	10.96	21.75	1.65	290.70	1.00	0.98
	2013LANÇA14S	0.86	7.75	21.75	1.65	366.30	1.00	0.98
	2013LANÇA15S	0.86	12.13	21.75	1.65	407.00	1.00	0.97
	2013LANÇA16S	0.86	9.33	21.75	1.65	465.10	1.00	0.95
	2013LANÇA17S	0.86	7.00	21.75	1.65	58.14	1.50	0.97
	2013LANÇA18S	0.86	7.00	21.75	1.65	87.21	1.51	0.97
	2013LANÇA19S	0.86	10.04	21.75	1.65	127.91	1.50	0.96
	2013LANÇA20S	0.86	11.13	21.75	1.65	186.05	1.41	1.00
	2013LANÇA21S	0.86	10.92	21.75	1.65	232.56	1.50	0.98

Table 1. Cont.

Authors	Run	$d_{50}$ (mm)	$t$ (Days)	$D^*$	$\rho'$	$D/d_{50}$	$h/D$	$u/u_c$
	2013LANÇA22S	0.86	9.21	21.75	1.65	290.70	1.50	0.96
	2013LANÇA23S	0.86	7.08	21.75	1.65	58.14	2.00	0.97
	2013LANÇA24S	0.86	7.04	21.75	1.65	87.21	2.00	0.97
	2013LANÇA25S	0.86	9.00	21.75	1.65	127.91	2.00	1.00
	2013LANÇA26S	0.86	13.75	21.75	1.65	186.05	1.88	0.98
	2013LANÇA27S	0.86	9.13	21.75	1.65	232.56	2.00	0.95
	2013LANÇA28S	0.86	7.00	21.75	1.65	58.14	2.50	0.97
	2013LANÇA29S	0.86	7.96	21.75	1.65	87.21	2.51	0.96
	2013LANÇA30S	0.86	7.67	21.75	1.65	127.91	2.50	0.98
	2013LANÇA31S	0.86	13.04	21.75	1.65	186.05	2.34	0.96
	2013LANÇA32S	0.86	7.21	21.75	1.65	58.14	3.00	0.96
	2013LANÇA33S	0.86	8.21	21.75	1.65	87.21	3.00	1.00
	2013LANÇA34S	0.86	7.04	21.75	1.65	127.91	3.00	0.96
	2013LANÇA35S	0.86	7.08	21.75	1.65	58.14	4.00	0.96
	2013LANÇA36S	0.86	13.08	21.75	1.65	87.21	4.00	0.98
	2013LANÇA37S	0.86	9.88	21.75	1.65	58.14	5.00	1.00
	2013LANÇA38S	0.86	13.13	21.75	1.65	87.21	5.00	0.96
Link et al. [22]	2017LINK01U	0.36	0.25	9.11	1.65	416.67	1.53	0.87
	2017LINK02U	0.36	1.78	9.11	1.65	416.67	1.60	0.99
Pizarro et al. [21]	2017PIZARRO01S	0.36	3.59	9.11	1.65	416.67	1.47	0.91
	2017PIZARRO02S	0.36	5.97	9.11	1.65	416.67	1.53	0.75
	2017PIZARRO01U	0.36	0.09	9.11	1.65	416.67	1.47	0.91
	2017PIZARRO02U	0.36	0.09	9.11	1.65	416.67	1.47	0.91
	2017PIZARRO03U	0.36	0.06	9.11	1.65	416.67	1.47	0.91
	2017PIZARRO04U	0.36	0.07	9.11	1.65	416.67	1.47	0.91
	2017PIZARRO05U	0.36	0.07	9.11	1.65	416.67	1.47	0.91
	2017PIZARRO06U	0.36	0.11	9.11	1.65	416.67	1.43	0.78

Note: Alabi [62] used  $u^*/u_c^*$ , instead of  $u/u_c$ .

The dataset is composed of natural and artificial sediments as well, with relative densities ranging from 0.04 to 1.65. The ratio between pier-diameter and sediment-size  $D/d_{50}$  ranges from 11.11 to 4159.09, and the ratio between flow-depth and pier-diameter takes values from 0.12 to 13.20.  $D^*$  ranges from 5.06 to 121.42 and thus covered flows with hydraulically smooth, transitional smooth-rough, and rough walls. The considered experimental data refer to clear-water conditions ( $u/u_c \leq 1$ ), allowing the identification of local scour without effects of overlapping processes, such as bedforms migration and scour hole refilling. Only four experiments are catalogued as exceptions to such decisions, in which their flow intensity values are slightly greater than one (2002OLIVETO18S, 2002OLIVETO33S, 1956CHABERT07S, and 1956CHABERT08S). Such exceptions were considered in order to have at least three experiments with the same  $D/d_{50}$  and different  $D^*$ , with the aim of analyzing the sediment and geometrical dependency on  $\lambda$  (Section 5.2.1).



**Figure 1.** Unsteady runs employed in this study. Images (a–f) are experiments 2005OLIVETO01U, 2005OLIVETO02U, 2005OLIVETO03U, 2005OLIVETO04U, 2005OLIVETO05U and 2005OLIVETO06U, respectively; images (g–l) are experiments 2017PIZARRO01U, 2017PIZARRO02U, 2017PIZARRO03U, 2017PIZARRO04U, 2017PIZARRO05U and 2017PIZARRO06U, respectively; and images (m,n) are experiments 2017LINK01U and 2017LINK02U, respectively.

4.2.  $Z_{max}^*$ ,  $W_{max}^*$ , and  $S$  Estimation

Sheppard et al. [9] evaluated 23 predictive equilibrium bridge scour depth formulations proposed for simple-shaped structures and founded in cohesionless sediments. The analyzed predictive methods were improved over time in terms of accuracy and the Sheppard/Melville (S/M) formulation was found to be the most accurate for the tested and considered dataset. Consequently, the S/M formulation was taken into account and slightly modified to estimate  $W_{max}^*$ ,  $Z_{max}^*$ , and  $S$ . Equations (18) to (21) present the original formulation,

$$\frac{z}{D} = 2.5f_1f_2f_3 \quad \text{for } 0.4 \leq \frac{u}{u_c} \leq 1.0 \tag{18}$$

$$f_1 = \tanh((h/D)^{0.4}) \tag{19}$$

$$f_2 = \left\{ 1 - 1.2[\ln(u/u_c)]^2 \right\} \tag{20}$$

$$f_3 = \left[ \frac{(D/d_{50})}{0.4(D/d_{50})^{1.2} + 10.6(D/d_{50})^{-0.13}} \right] \tag{21}$$

in which  $f_1$  represents the water depth effect on bridge pier scour,  $f_2$  the velocity influence, and  $f_3$  denotes scale effects between pier-diameter and sediment-size. Accordingly,  $f_1$  and  $f_2$  contain the hydraulic impacts on local scour, while  $f_3$  denotes scale ratio effects.

Note that the BRISENT model is able to reproduce the scour dynamic until the maximum selected value of  $W^*$ . Thus, it is convenient to choose its maximum value, i.e., relating  $W_{max}^*$  with  $W^*$  at equilibrium scour conditions. The laboratory data employed by Sheppard et al. [9] was used in correspondence with their formulation for estimating  $W_{max}^*$ ,  $S_{max}^*$ , and  $S$ . Such a dataset consists of 441 laboratory experiments and 791 field data. The original dataset was filtered by three conditions to ensure the calculation of  $W_{max}^* = W_{equilibrium}^*$ : (1) having complete information about the experiments; (2) clear-water scour; and (3)  $W_{max}^* \geq 1 \times 10^5$  in order to ensure the scour equilibrium state.

#### 4.3. Calibration and Validation Procedures

All  $\lambda$  fitting coefficients were determined by MATLAB(MathWorks, Natick, MA, USA) nonlinear curve-fit function, considering  $Z_{max}^*$  and  $W_{max}^*$  as the last measured point. Therefore,  $W_{max}^*$  and  $Z_{max}^*$  are not fitting coefficients when the BRISENT model is calibrated with time-dependent scour depth experiments; i.e., experiments that contain the whole scour depth evolution over time. The experiments are presented in Table 1.

Based on the unique relationship between  $W^*$  and  $Z^*$  (under clear-water conditions, constant sediment properties, and geometrical scales) [21], unsteady experiments were calibrated in two ways:

- Calibration employing unsteady data: Each unsteady run was calibrated with the aim of finding the best performance of the model. This kind of calibration will be called “unsteady calibration” in the rest of the paper.
- Calibration employing steady data: Two steady runs were used to calibrate the model with the aim of testing it in the most critical condition. The values of the dimensionless parameters regarding sediment properties and geometrical scale ( $D^*$ ,  $\rho'$ ,  $D/d_{50}$ ) are identical for calibration runs as well as for unsteady experiments, respectively. “2002OLIVETO32S” was used to calibrate Oliveto and Hager’s [19] unsteady runs and “2017PIZARRO01S” for the unsteady experiments of Pizarro et al. [21] and Link et al. [22]. This kind of calibration will be called “steady calibration” in the rest of the paper.

Table 2 summarizes calibration results for both calibration types.

**Table 2.** Steady and unsteady calibration of the BRISENT model.

Calibration Run	Model Parameter $\lambda$	RMSE (cm)
2005OLIVETO01U	486.63	0.27
2005OLIVETO02U	152.57	0.39
2005OLIVETO03U	105.38	0.52
2005OLIVETO04U	134.38	0.40
2005OLIVETO05U	246.28	0.34
2005OLIVETO06U	195.47	0.52
2017PIZARRO01U	2008.72	0.31
2017PIZARRO02U	1790.95	0.19
2017PIZARRO03U	2254.77	0.29
2017PIZARRO04U	1973.89	0.28
2017PIZARRO05U	1976.10	0.28
2017PIZARRO06U	1678.92	0.13
2002OLIVETO32S	280.9	0.76
2017PIZARRO01S	1078.86	0.40

Note: RMSE is defined as the root mean square error.

The BRISENT model is completely determined when  $\lambda$ ,  $Z_{max}^*$ , and  $W_{max}^*$  are known.  $Z_{max}^*$  and  $W_{max}^*$  are estimated employing the S/M formulation and the dataset of Sheppard et al. [9] in order to guarantee equilibrium conditions. This is a critical step for the proper use of the model due to Equation (11).

For validation procedures, the most complex experiments were used among those available to the authors: two highly unsteady and multi-peaked runs pertained to Link et al. [22] (2017LINK01U and 2017LINK02U).

## 5. Results

### 5.1. BRISENT as a Multipurpose Model

#### 5.1.1. BRISENT Performance under Steady Hydraulic Conditions

Ninety percent of the experimental data presented in Section 4 were performed under steady hydraulic conditions. Figure 2 illustrates the time-dependent scour depth for different experiments that consider the extreme values of the dimensionless parameters. In all cases, the BRISENT model is able to reproduce the scour evolution with root mean square error (RMSE) values between 0.04 and 1.60 cm. RMSE is defined as  $RMSE = \sqrt{\frac{1}{n} \sum_{j=1}^n (\hat{z}_j - z_j)^2}$ ; where  $z_j$  is the measured scour depth  $j$ ,  $\hat{z}_j$  is the computed scour depth  $j$ , and  $n$  is the number of measured points. Therefore, the proposed BRISENT model can reproduce the scour evolution with high accuracy under steady hydraulic conditions.

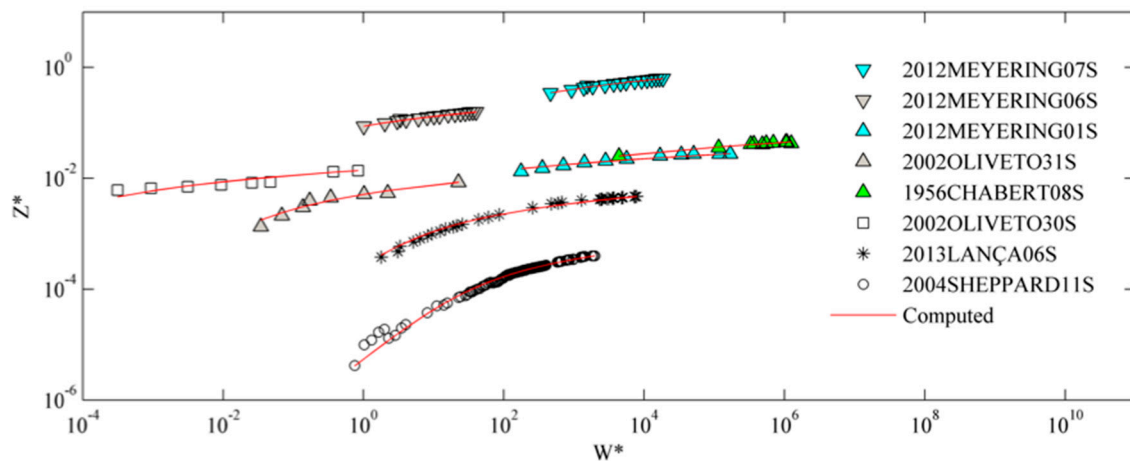


**Figure 2.** Measured (markers) and computed scour depth evolution using BRISENT model (red line) for experiments with extreme values of  $D^*$ ,  $\rho'$ ,  $D/d_{50}$ ,  $h/D$ , and  $u/u_c$ .

Note that the scour evolution presents similar behavior in two groups of experiments (triangle markers). The first group consists of the experiments “2012MEYERING06S” and “2012MEYERING07S”, while the second group consists of the experiments “2012MEYERING01S”, “2002OLIVETO31S”, and “1956CHABERT08S”. Such a similar scour evolution is due to the reduced variability of the dimensionless  $D/d_{50}$  that takes values around 10 and 120 for the first and second groups, respectively.

#### 5.1.2. BRISENT Performance under Flood Waves

Figure 3 presents the time-dependent evolution of the measured scour depth in contrast to the BRISENT model calibrated according to the procedure presented in Section 4.3. Table 3 summarizes the model benchmarking in terms of RMSE for each experiment. The results show that, independently of the kind of calibration, BRISENT correctly reproduces the time-dependent scour depth with RMSE values less than 1.57 and 0.52 cm for steady and unsteady calibrations, respectively.

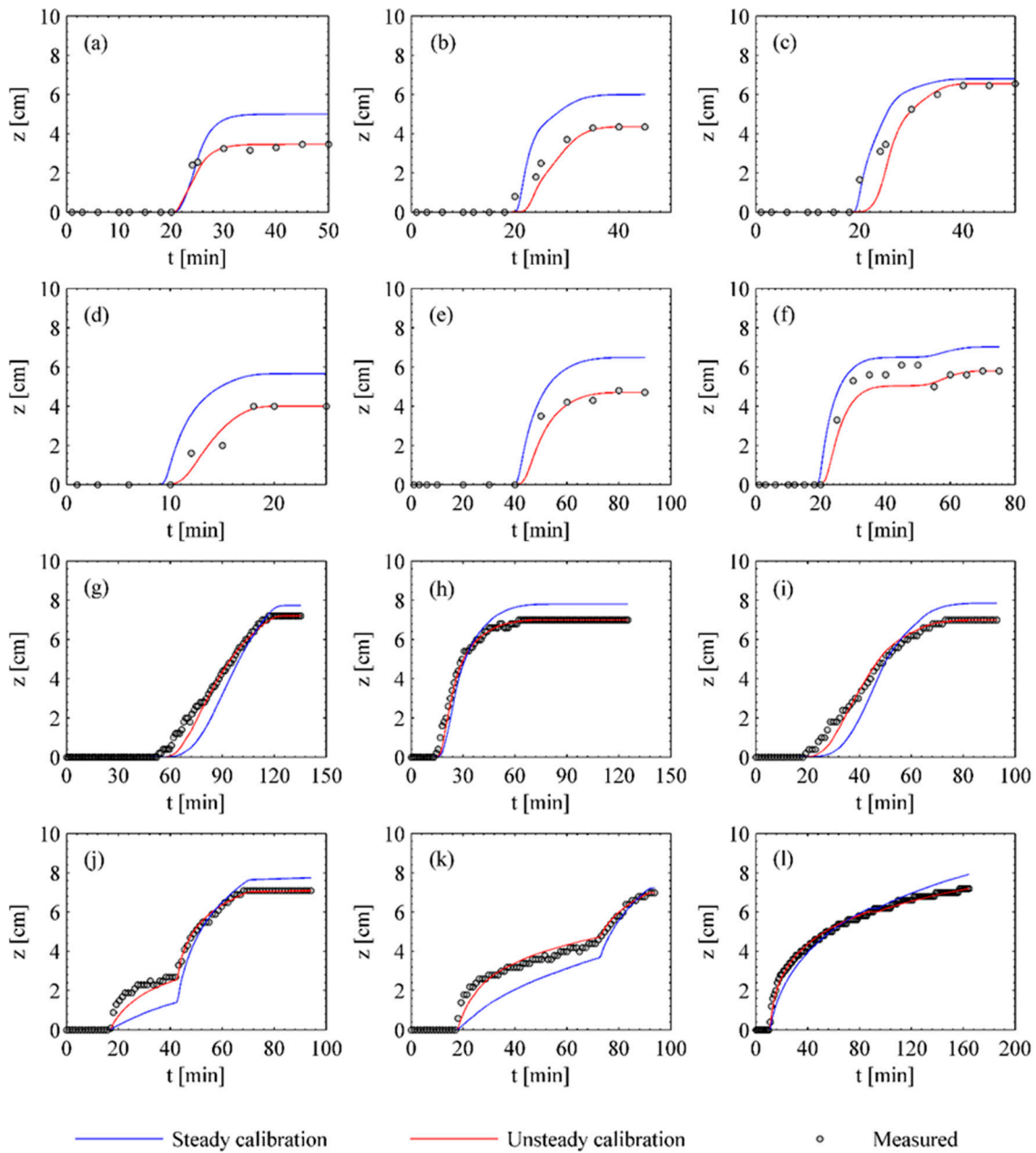


**Figure 3.** Benchmarking of the BRISENT model with  $\lambda$  calibrated with steady and unsteady runs. Images (a–f) are experiments 2005OLIVETO01U, 2005OLIVETO02U, 2005OLIVETO03U, 2005OLIVETO04U, 2005OLIVETO05U and 2005OLIVETO06U, respectively; images (g–l) are experiments 2017PIZARRO01U, 2017PIZARRO02U, 2017PIZARRO03U, 2017PIZARRO04U, 2017PIZARRO05U and 2017PIZARRO06U, respectively.

Steady calibration tends to overestimate the maximum scour depths after flood waves, while unsteady calibration presents better performances in all analyzed experiments. Furthermore, the average RMSE values are less than 1 cm, independently of the kind of calibration. Therefore, the proposed BRISENT model can reproduce the scour evolution with high accuracy under stepwise hydrographs and 100% unsteady hydraulic conditions.

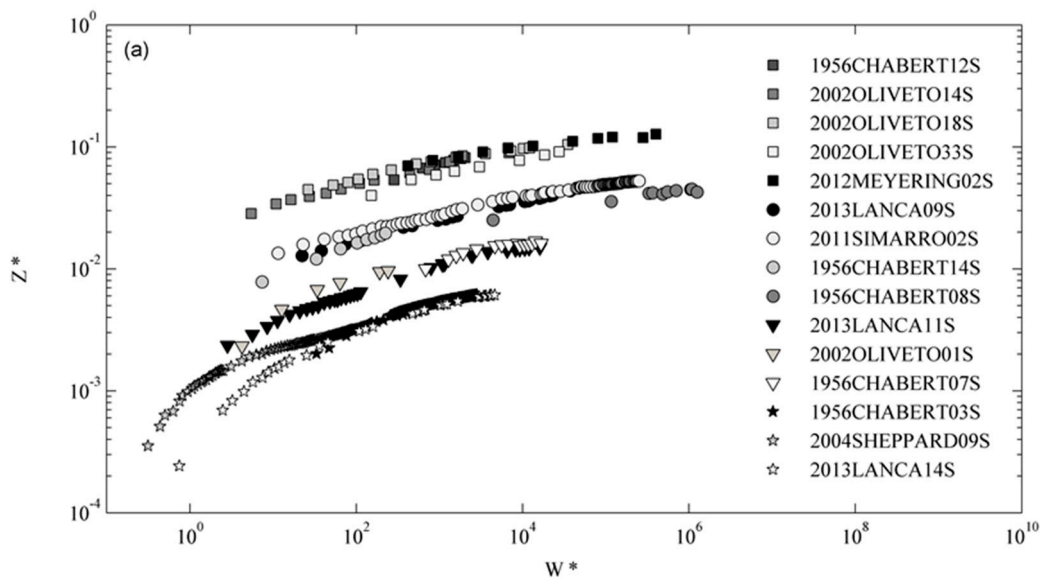
**Table 3.** Summary of model benchmarking in terms of RMSE.

Experimental Run	RMSE (cm)	
	Steady Calibration	Unsteady Calibration
2005OLIVETO01U	0.94	0.27
2005OLIVETO02U	1.17	0.39
2005OLIVETO03U	0.63	0.52
2005OLIVETO04U	1.57	0.40
2005OLIVETO05U	1.09	0.34
2005OLIVETO06U	0.83	0.52
2017PIZARRO01U	0.73	0.31
2017PIZARRO02U	0.71	0.19
2017PIZARRO03U	0.80	0.29
2017PIZARRO04U	0.82	0.28
2017PIZARRO05U	0.89	0.28
2017PIZARRO06U	0.42	0.13
Minimum	0.42	0.13
Maximum	1.57	0.52
Average	0.88	0.33

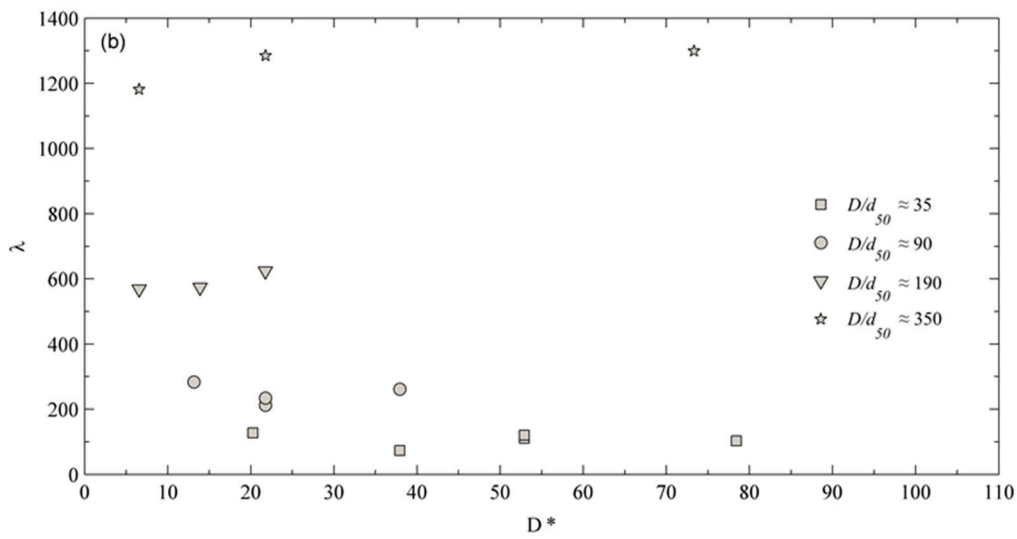
5.2. In Search of a Practical Formulation

5.2.1. Effects of  $D/d_{50}$  and  $D^*$  on  $\lambda$

A selected group of 15 experimental runs was considered to analyze the sediment and geometrical dependency on  $\lambda$ . This number was established in order to have at least three experiments with the same  $D/d_{50}$  and different  $D^*$ . The data were categorized in four classes depending on the geometrical scale between pier-diameter and sediment-size ( $D/d_{50} \approx 35, 90, 190,$  and  $350$ ). The range for the dimensionless particle diameter  $D^*$  takes values from 6.58 to 78.42. Figure 4a shows the evolution of  $Z^*$  over  $W^*$  according to the four  $D/d_{50}$  classes. All data collapse into a single and geometrically-dependent curve, independently of the hydraulic conditions.  $Z^*$  decreases with  $D/d_{50}$  for equal  $W^*$ .



**Figure 4.** Cont.



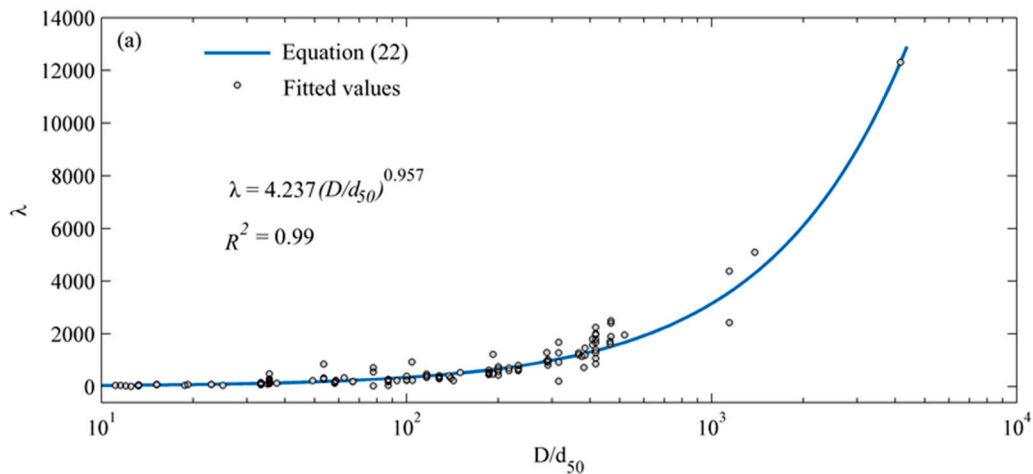
**Figure 4.** (a) Relative scour evolution over  $W^*$  for the four categorized classes; (b)  $\lambda$  calibrated values in function of the dimensionless particle diameter  $D^*$ .

Figure 4b shows calibrated  $\lambda$  on  $D^*$ . No correlation between these two variables is detected and it can be observed that  $\lambda$  is strongly controlled by  $D/d_{50}$ . A power function is adopted in order to describe this dependency:

$$\lambda = a_1 \left( \frac{D}{d_{50}} \right)^{a_2} \tag{22}$$

where  $a_1$  and  $a_2$  are fitting coefficients that were determined by the procedure presented in Section 4.3, obtaining  $a_1 = 4.237$  and  $a_2 = 0.957$  with a determination coefficient  $R^2 = 0.99$  and a RMSE equal to 49. Equation (22) is plotted in Figure 5a in comparison to the fitted values and Figure 5b presents the residuals between calibrated and estimated  $\lambda$ .

The fitting coefficient  $\lambda$  is always affected by the ratio between pier-diameter and sediment size, even for high values. Thus, a stabilizer or equilibrium threshold for it was not found.



**Figure 5.** Cont.

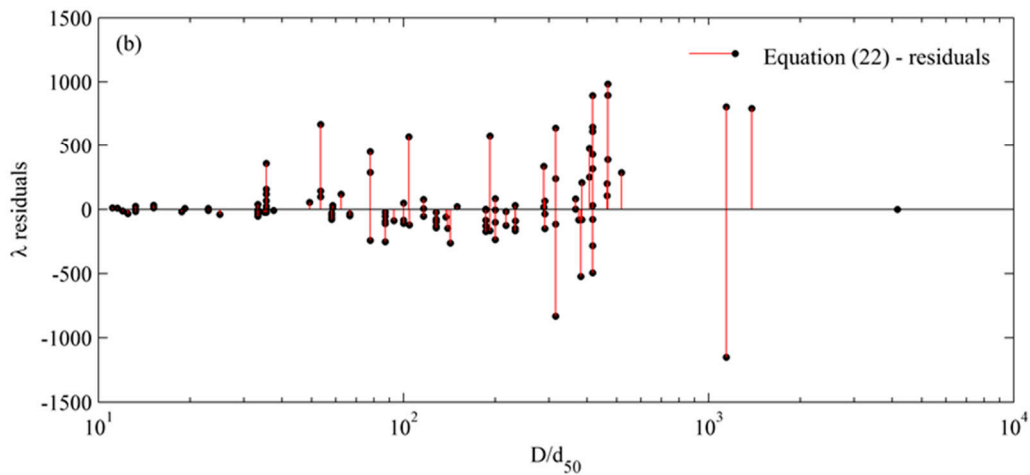


**Figure 5.** (a)  $\lambda$  values in function of  $D/d_{50}$ ; (b) Residual values for  $\lambda$  in comparison with estimated values using Equation (18).

5.2.2.  $Z^*$ ,  $W^*$ , and S Estimation

As mentioned in Section 4.2, the S/M formulation was taken into consideration and Equation (18) can be multiplied by  $2d_{50}/D$  in order to have  $Z^*$  on the left side of the equation,

$$Z^*_{max} = \frac{z}{D} \left( \frac{2d_{50}}{D} \right) = 2.5f_1f_2f_3 \left( \frac{2d_{50}}{D} \right) \tag{23}$$

The hydraulic effects in the original S/M formulation are represented by  $f_1$  and  $f_2$ . On the other hand,  $W^*$  has the capacity to integrate these hydraulic effects on the local scour process. Therefore,  $f_1$  and  $f_2$  can take a convenient value with the aim of writing it in a function of  $W^*_{max}$ . Considering  $f_1 = 1 = f_2$  makes it possible to be on the safe side from a design perspective and, consequently, this value was selected:

$$Z^*_{max} = 2.5 \left( \frac{2d_{50}}{D} \right) f_3 = \frac{5}{0.4(D/d_{50})^{1.2} + 10.6(D/d_{50})^{-0.13}} \tag{24}$$

From the experimental data of Sheppard et al. [9], only 129 of the total experiments were considered after applying the filters described in Section 4.3. Table 4 summarizes the source for laboratory data, the number of experiments from the source, and the range of selected dimensionless parameters according to the filtered dataset.

**Table 4.** Summary of the filtered experimental data. Data source: Sheppard et al. [9].

Author	Number of Runs	Range of Selected Dimensionless Parameters		
		$D/d_{50}$	$D^*$	$W^*_{max}$
Chiew (1984)	8	9.91–166.37	6.03–80.41	$6.89 \times 10^5$ – $3.16 \times 10^7$
Ettema (1980)	85	3.67–624.84	6.03–196.00	$1.22 \times 10^5$ – $4.78 \times 10^8$
Ettema and others (2006)	4	60.96–229.62	26.39–26.39	$1.15 \times 10^5$ – $1.63 \times 10^6$
Graf (1995)	3	47.61–71.41	52.77–52.77	$4.17 \times 10^6$ – $9.25 \times 10^6$
Jones (unpublished)	8	30.36–505.97	7.54–125.64	$1.25 \times 10^5$ – $5.27 \times 10^6$
Melville (1997)	4	19.81–31.24	20.10–20.10	$3.04 \times 10^5$ – $4.16 \times 10^6$
Melville and Chiew (1999)	9	39.69–73.03	24.12–24.12	$1.02 \times 10^5$ – $2.26 \times 10^6$
Sheppard and others (2004)	8	142.49–4159.13	5.53–72.87	$1.26 \times 10^5$ – $7.63 \times 10^5$

$W_{max}^*$  versus  $D/d_{50}$  values are plotted in Figure 6, in which the solid line represents Equation (25):

$$\ln W_{max}^* = a \left( \ln \frac{D}{d_{50}} \right)^b \tag{25}$$

where  $a$  and  $b$  are fitting coefficients that were calibrated by the procedure described in Section 4.3, obtaining  $a = 21.84$  and  $b = -0.295$  with a determination coefficient  $R^2 = 0.65$  and a RMSE = 1.19.

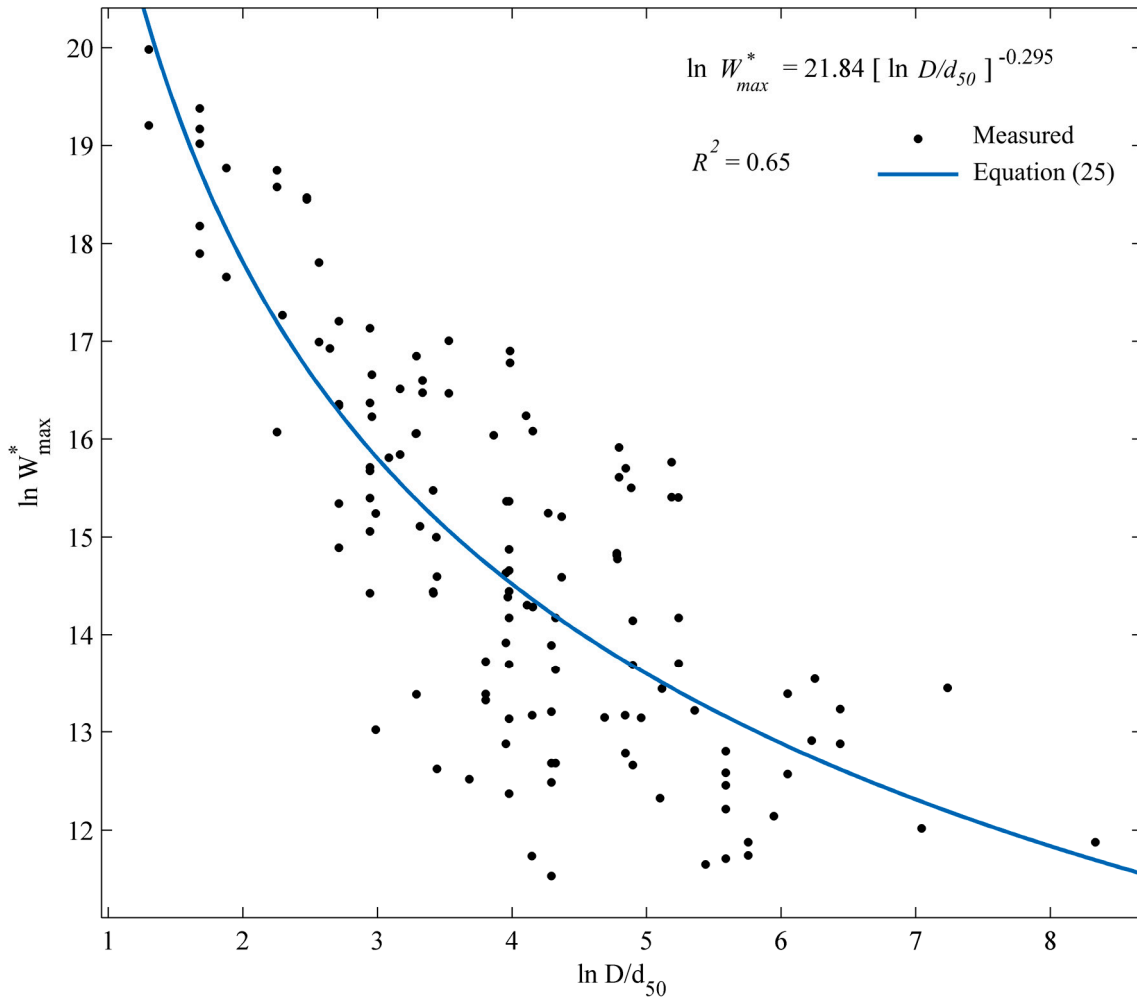


**Figure 6.**  $W_{max}^*$  versus  $D/d_{50}$  values for the filtered dataset in comparison with the fitting function Equation (25). Data source: Sheppard et al. [9].

Therefore,  $W_{max}^*$  can be evaluated by Equation (26) and the entropic scour parameter  $S$  can be estimated with Equation (27) (Equation (13) in combination with Equation (24)):

$$W_{max}^* = \exp \left[ 21.84 \left( \ln \frac{D}{d_{50}} \right)^{-0.295} \right] \tag{26}$$

$$S = \frac{21.185(D/d_{50})^{0.957}}{0.4(D/d_{50})^{1.2} + 10.6(D/d_{50})^{-0.13}} \tag{27}$$

### 5.3. BRISENT Validation: Highly Unsteady and Multi-Peaked Hydrographs

The BRISENT model was validated using highly unsteady and multi-peaked hydrographs pertaining to Link et al. [22]. Validation runs are plotted on Figure 7a–d, presenting the time-dependent evolution of the measured scour depth in contrast to the BRISENT model calibrated and estimated according to the proposed equations (Equations (22), (26) and (27)).

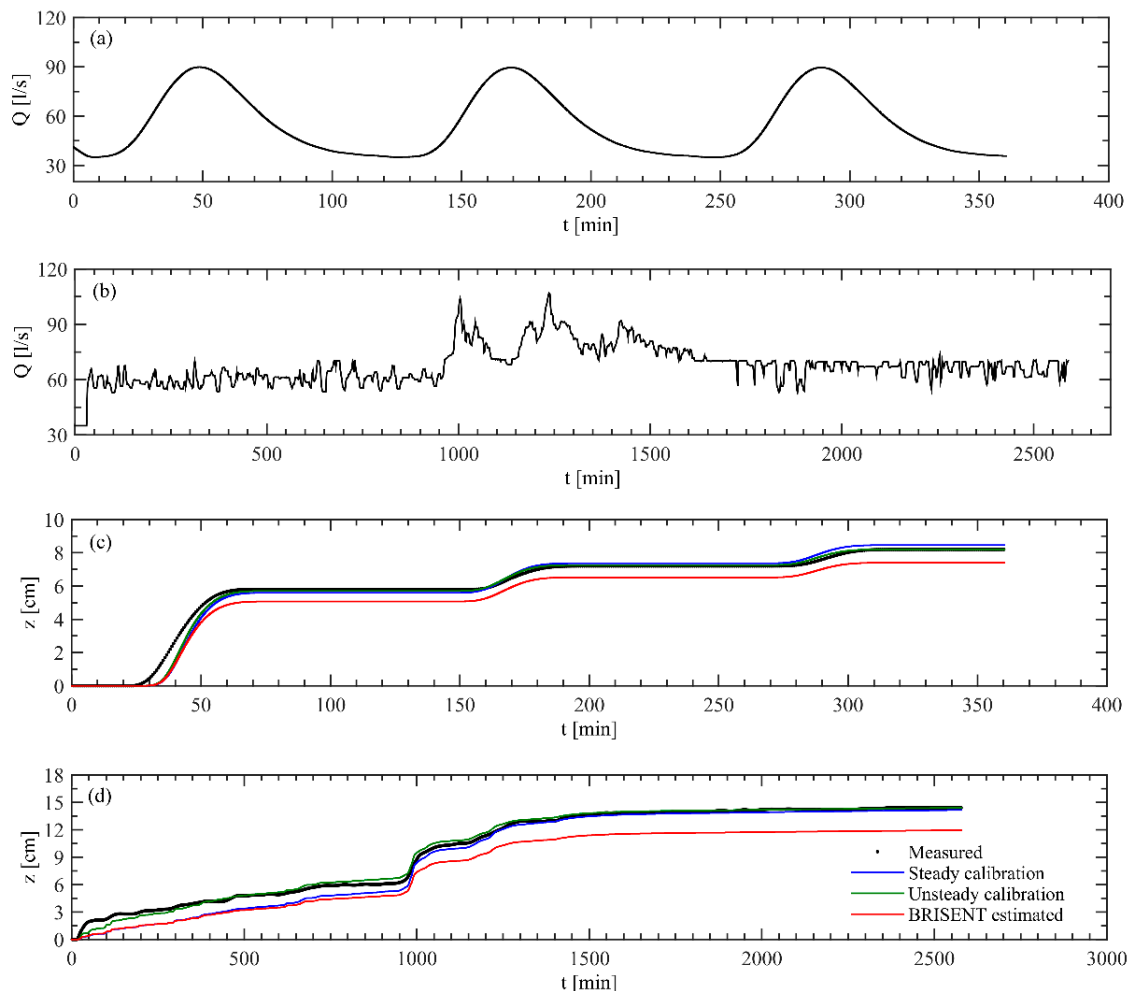


**Figure 7.** Validation of the BRISENT model with highly unsteady experiments. Images (a,b) are experiments 2017LINK01U and 2017LINK02U, respectively. Images (c,d) present measured scour depths over time, BRISENT model calibrated using a steady run, BRISENT model calibrated using unsteady runs, and BRISENT model considering Equation (13) to Equation (14) and Equation (19) to Equation (22) for experiments 2017LINK01U and 2017LINK02U, respectively.

Table 5 summarizes the model benchmarking in terms of RMSE for experiments “2017LINK01U” and “2017LINK02U”, and the results show that the proposed equations correctly reproduce the main dynamic of the time-dependent scour depth. Note that the unsteady calibration provides the most accurate results with RMSE values less than 0.32 cm, while the observed higher RMSE values for the estimated BRISENT model rely on the computed values of  $Z_{max}^*$ . Steady calibration shows good performance as well, with RMSE values less than 0.81 cm.

**Table 5.** Summary of model benchmarking in terms of RMSE.

	Calibration Run	Model Parameter $\lambda$	2017LINK01U	2017LINK02U
			RMSE (cm)	RMSE (cm)
Steady calibration	2017PIZARRO01S	1078.86	0.35	0.81
Unsteady calibration	2017LINK01U and 2017LINK02U, respectively	1391.84 and 1284.06, respectively	0.21	0.32
BRISSENT estimated	—	1362.06	0.72	2.01

## 6. Discussion

### 6.1. Informational Entropy and the Principle of Maximum Entropy for Pier Scour Modelling

From a practical perspective, traditional bridge scour formulas are used in order to estimate a potential scour depth that could occur during bridge life. However, neither a vectorial nor an empirical approach can estimate the scour process by considering long duration events, discharge regime, and the interactions of different erosional processes. Therefore, scour depth estimations are uncertain.

The informational entropy concept has long been recognized as a measure of uncertainties, and is the ideal concept for analyzing the bridge scour phenomenon. Moreover, BRISSENT is based on the effective flow work parameter ( $W^*$ ) and thus, the combination of  $W^*$  and the principle of maximum entropy (POME) is a variational/thermodynamic approach for treating the scour process. The fact that the core of the model is based on the informational entropy concept (uncertainty) presents a clear advantage in comparison to other formulations by taking into consideration bridge design, bridge life, and hydrologic regime.

### 6.2. BRISSENT: A Multipurpose Model

BRISSENT was inferred without imposing the hydraulic conditions, under which the model can run. In particular, the results confirm that the BRISSENT model can be used under different and complex hydraulic conditions (steady flows, step-wise hydrographs, and flood waves with multi-peaked hydrographs) to describe bridge scour phenomena, and independently of the type of calibration. In consequence, BRISSENT can be considered a multipurpose model which allows calibration under simple hydraulic conditions and application to more complex and realistic hydraulic situations. Since, in the past, most scour experiments were carried out under steady hydraulic conditions, these are clear advantages over other published formulations.

### 6.3. Wide Range of the Considered Dimensionless Parameters

Two hundred and sixty-six clear-water scour experiments were considered for the calibration process, with widely ranging dimensionless parameters. For example,  $D^*$  ranges from 5.06 to 121.42 and, thus, covered flows with hydraulically smooth, transitional smooth-rough, and rough walls, according to Oliveto and Hager [66]. The ratio between pier-diameter and sediment-size  $D/d_{50}$  ranges from 11.11 to 4159.09 and, thus, the obtained results can be used in both laboratory and natural scales. The same can be said for the ratio between flow-depth and pier-diameter, which takes values from 0.12 to 13.20.

### 6.4. Applicability of the Model: Advantages and Limitations

Simple equations are proposed to estimate the time-dependent scour depth independently of hydraulic conditions, geometrical scale, and hydraulic flow roughness. Equation (26) and Equation (27) are empiric equations for  $S$  and  $W_{max}^*$  which are based on the dataset published by Sheppard et al. [9]. Such dataset contains a wide value range of dimensionless parameters, making it possible to

treat the bridge scour phenomenon under different flow regimes and different geometrical scales. Furthermore, the results show that the proposed equations correctly reproduce the main dynamic of the time-dependent scour depth under clear-water conditions, where no overlapping of other erosional processes occur.

#### 6.5. Key Dimensionless Parameters: $W^*$ and $D/d_{50}$

The ratio between pier-diameter and sediment-size (geometrical scale) is the most critical physical characteristic controlling the scour model parametrization. From a physical modeling perspective, keeping constant a high value of  $D/d_{50}$  at laboratory scales is very hard due to the sediment cohesion (sediment size has to be reduced 10 times or more in laboratory flumes). As a consequence, theoretical efforts to develop new and more accurate models are a major challenge in this field, where the BRISENT model represents the first model of its kind. Additionally, our results highlight that the key dimensionless parameters are  $W^*$  and  $D/d_{50}$ . Such parameters contain the energy for undermining and the geometrical scale between pier diameter and sediment size, respectively. More energy to reach the same relative scour depth at a real scale was observed, thus positioning laboratory-deduced formulas on the side of safety from a design perspective.

### 7. Conclusions

Bridge-pier scour evolution has been analyzed in the present work, using the first mathematical formulation for simulating scour phenomena based on energy concepts and entropy theory. The proposed BRISENT model has been established on the effective flow work parameter ( $W^*$ ) and on the principle of maximum entropy (POME). The results confirm the idea that the local-scour phenomenon indirectly depends on the time-dependent mean velocity, and thus the model can be calibrated using steady scour data and applied to more complex hydraulic scenarios. Literature data under clear-water conditions were employed, in which the key dimensionless parameters took values over a wide range, allowing analysis of the local scour phenomenon from a holistic point of view. Simple formulations were proposed to estimate the fitting coefficient  $\lambda$  (Equation (22)) and the entropic-scour parameter  $S$  (Equation (27)). Moreover, we observed that the ratio  $D/d_{50}$  is the most critical physical characteristic controlling the scour model parametrization.

Our results support the idea that POME and  $W^*$  could be used to explain erosional processes and, in particular, to describe clear-water local-scour phenomena with high accuracy and simple formulations. This is an entry point for treating more complex river interaction processes at different spatial scales (e.g., channel instability, channel bed gradation, channel migration, contraction scour, local scour, etc.). The authors are keen to apply these concepts with the aim of answering the following questions: (i) how long does it take to reach the equilibrium state under clear-water, bed-load, suspension conditions and/or a possible combination of scour modes at real piers? (ii) is it achievable during the lifetime of bridges? (iii) how does the scour-hole refilling process affect the whole scour dynamic? (iv) what is the time-evolution of  $W^*$  and  $Z^*$ ?

**Acknowledgments:** The authors would like to thank Professor Giuseppe Oliveto (University of Basilicata) for providing his experimental data, and the support of the European Commission under the ELARCH program (Project Reference number: 552129-EM-1-2014-1-IT-ERA MUNDUS-EMA21). OL thanks the Chilean Research Council CONICYT for the research project FONDECYT 1150997 "Bridge pier scour under flood waves". This publication reflects the authors' view only and the Commission is not liable for any use that may be made of the information contained therein. The constructive comments of four anonymous reviewers are gratefully appreciated and the review comments helped to substantially improve the paper. This work was carried out within the scientific agreement between the Civil Protection of Basilicata, the CINID and the University of Basilicata for the startup of the Functional Center of Basilicata.

**Author Contributions:** All authors made a substantial contribution to this paper. A.P. conceived the model, wrote the first draft, and submitted the manuscript. M.F. added entropic ideas to the study. C.S. contributed to the data analysis and improvement of the document. O.L. and S.M. designed and mentored the research and contributed to the results interpretation.

**Conflicts of Interest:** The authors declare no conflict of interest.

## References

- Briaud, J.L.; Brandimarte, L.; Wang, J.; D’Odorico, P. Probability of scour depth exceedance owing to hydrologic uncertainty. *Georisk Assess. Manag. Risk Eng. Syst. Geohazards* **2007**, *1*, 77–88. [[CrossRef](#)]
- Cook, W. *Bridge Failure Rates, Consequences, and Predictive Trends*; Utah State University: Logan, UT, USA, 2014; ISBN 1321576021.
- Imam, B.M.; Marios, K. Causes and consequences of metallic bridge failures. *Struct. Eng. Int.* **2012**, *22*, 93–98. [[CrossRef](#)]
- Kattell, J.; Eriksson, M. *Bridge Scour Evaluation: Screening, Analysis, & Countermeasures*; San Dimas Technology and Development Center: San Dimas, CA, USA, 1998.
- Smith, D.W. Bridge failures. *Proc. Inst. Civ. Eng.* **1976**, *60*, 367–382. [[CrossRef](#)]
- Wardhana, K.; Hadipriono, F.C. Analysis of recent bridge failures in the United States. *J. Perform. Constr. Facil.* **2003**, *17*, 144–150. [[CrossRef](#)]
- Melville, B.W. Pier and abutment scour: Integrated approach. *J. Hydraul. Eng.* **1997**, *123*, 125–136. [[CrossRef](#)]
- Richardson, E.V.; Davis, S.R. *Evaluating Scour at Bridges: Hydraulic Engineering Circular No. 18*; Federal Highway Administration: Washington, DC, USA, 1995.
- Sheppard, D.M.; Melville, B.; Demir, H. Evaluation of Existing Equations for Local Scour at Bridge Piers. *J. Hydraul. Eng.* **2014**, *140*, 14–23. [[CrossRef](#)]
- Zanke, U. *Kolke am Pfeiler in richtungskonstanter Strömung und unter Welleneinfluss*; Universität Hannover: Hannover, Germany, 1982; Volume 54, pp. 381–416.
- Manes, C.; Brocchini, M. Local scour around structures and the phenomenology of turbulence. *J. Fluid Mech.* **2015**, *779*, 309–324. [[CrossRef](#)]
- Dey, S. Time-variation of scour in the vicinity of circular piers. *Proc. Inst. Civ. Eng. Marit. Energy* **1999**, *136*, 67–75. [[CrossRef](#)]
- Melville, B.W.; Chiew, Y.-M. Time scale for local scour at bridge piers. *J. Hydraul. Eng.* **1999**, *125*, 59–65. [[CrossRef](#)]
- Oliveto, G.; Hager, W.H. Temporal evolution of clear-water pier and abutment scour. *J. Hydraul. Eng.* **2002**, *128*, 811–820. [[CrossRef](#)]
- Sheppard, D.M.; Miller, W., Jr. Live-bed local pier scour experiments. *J. Hydraul. Eng.* **2006**, *132*, 635–642. [[CrossRef](#)]
- Lai, J.-S.; Chang, W.-Y.; Yen, C.-L. Maximum local scour depth at bridge piers under unsteady flow. *J. Hydraul. Eng.* **2009**, *135*, 609–614. [[CrossRef](#)]
- Kothyari, U.C.; Garde, R.C.J.; Ranga Raju, K.G. Temporal variation of scour around circular bridge piers. *J. Hydraul. Eng.* **1992**, *118*, 1091–1106. [[CrossRef](#)]
- López, G.; Teixeira, L.; Ortega-Sánchez, M.; Simarro, G. Estimating final scour depth under clear-water flood waves. *J. Hydraul. Eng.* **2014**, *140*, 328–332. [[CrossRef](#)]
- Oliveto, G.; Hager, W.H. Further results to time-dependent local scour at bridge elements. *J. Hydraul. Eng.* **2005**, *131*, 97–105. [[CrossRef](#)]
- Hager, W.H.; Unger, J. Bridge pier scour under flood waves. *J. Hydraul. Eng.* **2010**, *136*, 842–847. [[CrossRef](#)]
- Pizarro, A.; Ettmer, B.; Manfreda, S.; Rojas, A.; Link, O. Dimensionless effective flow work for estimation of pier scour caused by flood waves. *J. Hydraul. Eng.* **2017**, *143*. [[CrossRef](#)]
- Link, O.; Castillo, C.; Pizarro, A.; Rojas, A.; Ettmer, B.; Escauriaza, C.; Manfreda, S. A model of bridge pier scour during flood waves. *J. Hydraul. Res.* **2017**, *55*. [[CrossRef](#)]
- Sturm, T.; Sotiropoulos, F.; Landers, M.; Gotvald, T.; Lee, S.; Ge, L.; Navarro, R.; Escauriaza, C. Laboratory and 3D numerical modeling with field monitoring of regional bridge scour in Georgia. In *Georgia Department of Transportation Final Project*; Georgia Dept. of Transportation: Atlanta, GA, USA, 2004.
- Clubley, S.K.; Manes, C.; Richards, D.J. High resolution sonars set to revolutionise bridge scour inspections. *Proc. Inst. Civ. Eng. Civ. Eng.* **2015**, *168*, 35–42. [[CrossRef](#)]
- Prendergast, L.J.; Gavin, K. A review of bridge scour monitoring techniques. *J. Rock Mech. Geotech. Eng.* **2014**, *6*, 138–149. [[CrossRef](#)]
- Hong, J.-H.; Guo, W.-D.; Chiew, Y.-M.; Chen, C.-H. A new practical method to simulate flood-induced bridge pier scour—A case study of Mingchu bridge piers on the Cho-Shui River. *Water* **2016**, *8*, 238. [[CrossRef](#)]

27. Su, C.-C.; Lu, J.-Y. Comparison of Sediment Load and Riverbed Scour during Floods for Gravel-Bed and Sand-Bed Reaches of Intermittent Rivers: Case Study. *J. Hydraul. Eng.* **2016**, *142*, 5016001. [[CrossRef](#)]
28. Gaudio, R.; Grimaldi, C.; Tafarojnoruz, A.; Calomino, F. Comparison of formulae for the prediction of scour depth at piers. In Proceedings of the 1st IAHR European Division Congress, Edinburgh, UK, 4–6 May 2010.
29. Gaudio, R.; Tafarojnoruz, A.; De Bartolo, S. Sensitivity analysis of bridge pier scour depth predictive formulae. *J. Hydroinform.* **2013**, *15*, 939–951. [[CrossRef](#)]
30. Barbe, D.E.; Cruise, J.F.; Singh, V.P. Probabilistic approach to local bridge pier scour. *Transp. Res. Rec. 1350* **1992**, 28–33. Available online: <https://trid.trb.org/view.aspx?id=370731> (accessed on 5 November 2017).
31. Johnson, P.A. Reliability-based pier scour engineering. *J. Hydraul. Eng.* **1992**, *118*, 1344–1358. [[CrossRef](#)]
32. Johnson, P.A. Fault tree analysis of bridge failure due to scour and channel instability. *J. Infrastruct. Syst.* **1999**, *5*, 35–41. [[CrossRef](#)]
33. Johnson, P.A.; Ayyub, B.M. Assessing time-variant bridge reliability due to pier scour. *J. Hydraul. Eng.* **1992**, *118*, 887–903. [[CrossRef](#)]
34. Johnson, P.A.; Ayyub, B.M. Modeling uncertainty in prediction of pier scour. *J. Hydraul. Eng.* **1996**, *122*, 66–72. [[CrossRef](#)]
35. Johnson, P.A.; Hell, T.M. Bridge Scour-A Probabilistic Approach. *Infrastruct. Sussex* **1996**, *1*, 24–30.
36. Johnson, P.A.; Dock, D.A. Probabilistic bridge scour estimates. *J. Hydraul. Eng.* **1998**, *124*, 750–754. [[CrossRef](#)]
37. Yanmaz, A.M.; Cicekdag, O. Composite reliability model for local scour around cylindrical bridge piers. *Can. J. Civ. Eng.* **2001**, *28*, 520–535. [[CrossRef](#)]
38. Yanmaz, A.M.; Üstün, I. Generalized reliability model for local scour around bridge piers of various shapes. *Turk. J. Eng. Environ. Sci.* **2001**, *25*, 687–698.
39. Johnson, P.A.; Clopper, P.E.; Zevenbergen, L.W.; Lagasse, P.F. Quantifying uncertainty and reliability in bridge scour estimations. *J. Hydraul. Eng.* **2015**, *141*, 4015013. [[CrossRef](#)]
40. Flint, M.M.; Fringer, O.; Billington, S.L.; Freyberg, D.; Diffenbaugh, N.S. Historical Analysis of Hydraulic Bridge Collapses in the Continental United States. *J. Infrastruct. Syst.* **2017**, *23*, 4017005. [[CrossRef](#)]
41. Robinson, D.W. Entropy and uncertainty. *Entropy* **2008**, *10*, 493–506. [[CrossRef](#)]
42. Wang, Q.A. Probability distribution and entropy as a measure of uncertainty. *J. Phys. A Math. Theor.* **2008**, *41*, 65004. [[CrossRef](#)]
43. Koutsoyiannis, D. Entropy: From thermodynamics to hydrology. *Entropy* **2014**, *16*, 1287–1314. [[CrossRef](#)]
44. Dong, X.; Lu, H.; Xia, Y.; Xiong, Z. Decision-Making Model under Risk Assessment Based on Entropy. *Entropy* **2016**, *18*, 404. [[CrossRef](#)]
45. Kvålseth, T.O. On the measurement of randomness (uncertainty): A more informative entropy. *Entropy* **2016**, *18*, 159. [[CrossRef](#)]
46. Jaynes, E.T. Information theory and statistical mechanics. II. *Phys. Rev.* **1957**, *108*, 171. [[CrossRef](#)]
47. Chiu, C.-L. Entropy and probability concepts in hydraulics. *J. Hydraul. Eng.* **1987**, *113*, 583–599. [[CrossRef](#)]
48. Fiorentino, M.; Claps, P.; Singh, V.P. An entropy-based morphological analysis of river basin networks. *Water Resour. Res.* **1993**, *29*, 1215–1224. [[CrossRef](#)]
49. Singh, V.P. Entropy theory for movement of moisture in soils. *Water Resour. Res.* **2010**, *46*, W0516. [[CrossRef](#)]
50. Singh, V.P. Entropy theory for derivation of infiltration equations. *Water Resour. Res.* **2010**, *46*, W03527. [[CrossRef](#)]
51. Singh, V.P. *Entropy Theory in Hydraulic Engineering: An Introduction*; American Society of Civil Engineers: Reston, VA, USA, 2014. [[CrossRef](#)]
52. Singh, V.P. *Entropy Theory in Hydrologic Science and Engineering*; McGraw Hill Professional: New York, NY, USA, 2014; ISBN 0071835474.
53. Moramarco, T.; Corato, G.; Melone, F.; Singh, V.P. An entropy-based method for determining the flow depth distribution in natural channels. *J. Hydrol.* **2013**, *497*, 176–188. [[CrossRef](#)]
54. Hemelrijk, J. Underlining random variables. *Stat. Neerl.* **1966**, *20*, 1–7. [[CrossRef](#)]
55. Breusers, H.N.C.; Nicollet, G.; Shen, H.W. Local scour around cylindrical piers. *J. Hydraul. Res.* **1977**, *15*, 211–252. [[CrossRef](#)]
56. May, R.W.P.; Willoughby, I.R. *Local Scour around Large Obstructions*; Technical Report; Hydraulics Research: Wallingford, Oxfordshire, UK, 1990.
57. Miller, W., Jr.; Sheppard, D.M. Time rate of local scour at a circular pile. In Proceedings of the First International Conference on Scour of Foundations, College Station, TX, USA, 17–20 November 2002.

58. Chabert, J.; Engeldinger, P. *Etude des Affouillements Autour des Piles des Ponts*; Laboratoire National d'Hydraulique: Chatou, France, 1956; p. 118. (In French)
59. Franzetti, S.; Larcán, E.; Mignosa, P. Erosione alla base di pile circolari di ponte: Verifica sperimentale dell'ipotesi di esistenza di una situazione finale di equilibrio. *Idrotecnica* **1989**, *16*, 135–141.
60. Sheppard, D.M.; Odeh, M.; Glasser, T. Large scale clear-water local pier scour experiments. *J. Hydraul. Eng.* **2004**, *130*, 957–963. [[CrossRef](#)]
61. Grimaldi, C. Non-Conventional Countermeasures Against Local Scouring at Bridge Piers. Ph.D. Thesis, The Hydraulic Engineering for Environment and Territory University, Cosenza, Italy, 2005.
62. Alabi, P.D. Time Development of Local Scour at a Bridge Pier Fitted with a Collar. Master's Thesis, University of Saskatchewan, Saskatoon, SK, Canada, 2006.
63. Simarro, G.; Fael, C.M.S.; Cardoso, A.H. Estimating equilibrium scour depth at cylindrical piers in experimental studies. *J. Hydraul. Eng.* **2011**, *137*, 1089–1093. [[CrossRef](#)]
64. Meyering, H. Effect of Sediment Density in Bridge Pier Scour Experiments. Ph.D. Thesis, Technical University of Braunschweig, Braunschweig, Germany, 2012.
65. Lança, R.M.; Fael, C.S.; Maia, R.J.; Pêgo, J.P.; Cardoso, A.H. Clear-water scour at comparatively large cylindrical piers. *J. Hydraul. Eng.* **2013**, *139*, 1117–1125. [[CrossRef](#)]
66. Giuseppe, O.; Hager, H.W. Closure to "Further Results to Time-Dependent Local Scour at Bridge Elements" by Giuseppe Oliveto and Willi H. Hager. *J. Hydraul. Eng.* **2006**, *132*, 997–998. [[CrossRef](#)]



© 2017 by the authors. Licensee MDPI, Basel, Switzerland. This article is an open access article distributed under the terms and conditions of the Creative Commons Attribution (CC BY) license (<http://creativecommons.org/licenses/by/4.0/>).